Collective phenomena emerging from the interactions between dynamical processes in multiplex networks

Vincenzo Nicosia,[1] Per Sebastian Skardal,[2] Alex Arenas,[3] and Vito Latora[1,4]

[1] *School of Mathematical Sciences, Queen Mary University of London, London E1 4NS, United Kingdom*
[2] *Department of Mathematics, Trinity College, Hartford, CT 06106, USA*
[3] *Department d'Enginyeria Informática i Matemátiques, Universitat Rovira i Virgili, 43007 Tarragona, Spain*
[4] *Dipartimento di Fisica ed Astronomia, Università di Catania and INFN, I-95123 Catania, Italy*

We introduce a framework to intertwine dynamical processes of different nature, each with its own distinct network topology, using a multilayer network approach. As an example of collective phenomena emerging from the interactions of multiple dynamical processes, we study a model where neural dynamics and nutrient transport are bidirectionally coupled in such a way that the allocation of the transport process at one layer depends on the degree of synchronization at the other layer, and vice versa. We show numerically, and we prove analytically, that the multilayer coupling induces a spontaneous explosive synchronization and a heterogeneous distribution of allocations, otherwise not present in the two systems considered separately. Our framework can find application to other cases where two or more dynamical processes such as synchronization, opinion formation, information diffusion, or disease spreading, are interacting with each other.

Networks are a powerful way to model and study a wide variety of complex phenomena [1, 2]. In the recent years, the study of collective dynamical processes on complex networks has improved our understanding of many complex systems and shed light on a wide range of physical, biological and social phenomena including synchronization [3], disease spreading [4], transport [5] and cascades [6]. Of particular interest in these works is the interplay between the structure of the network and its dynamics [7, 8]. In fact, the topology of a network has an effect on the dynamical processes that take place over the network [9], while some properties of the dynamics can reveal important information on the interaction network [10–12]. Understanding the relations between structure and dynamics can provide a solid foundation for modeling, predicting, and controlling dynamical processes in the real world. However, save for a few notable exceptions [13–15], the majority of the studies so far have considered a single process on a single network, ignoring a very important ingredient: often the components of a complex system interact through two or more dynamics at the same time, and these dynamics usually depend on each other in highly non-trivial ways.

In this Letter we propose a general framework for modelling, through a multiplex network, the *coupling of dynamical processes* of the same type (e.g. the spreading of two coupled diseases) or of different types (for instance a synchronization dynamics and a diffusion process). Moreover, we demonstrate with a specific example that this coupling mechanism can give rise to the emergence of complex phenomena generated by the interactions between the different dynamical processes.

The natural way to consider M interacting dynamical processes taking place over a complex system is to use a multiplex network with M layers [16–19]. Each layer contains the same number of nodes, N, and there exists a one-to-one correspondence between nodes in different layers, but the topology and the very same nature of the connections at each layer may be different. We then assign a different dynamical process to each layer. Considering for simplicity the case $M = 2$, we assume that the dynamics of the entire system is governed by the following equations:

$$\begin{cases} \dot{x}_i = F_{\omega_i}(\mathbf{x}, A^{[1]}) \\ \dot{y}_i = G_{\chi_i}(\mathbf{y}, A^{[2]}) \end{cases} \qquad i = 1, 2, \dots N \tag{1}$$

where $\mathbf{x} = \{x_1, x_2, \dots, x_N\} \in \mathbb{R}^N$ and $\mathbf{y} = \{y_1, y_2, \dots, y_N\} \in \mathbb{R}^N$ denote the states of the two dynamical processes, while the topologies of the two layers are encoded in the adjacency matrices $A^{[1]} = \{a_{ij}^{[1]}\}$ and $A^{[2]} = \{a_{ij}^{[2]}\}$ respectively, such that $a_{ij}^{[1]} = 1$ ($a_{ij}^{[2]} = 1$) if a link exists between nodes i and j in the first (second) layer, and $a_{ij}^{[1]} = 0$ ($a_{ij}^{[2]} = 0$) otherwise. The dynamical evolution of the two network processes is ruled respectively by the functions F_ω and G_χ, which depend on the sets of parameters ω and χ, so that the state x_i (y_i) of node i at the first (second) layer is a function of the state $\mathbf{x}$ ($\mathbf{y}$) and of the topology $A^{[1]}$ ($A^{[2]}$) of the first (second) layer. The key ingredient that connects the two dynamical processes is provided by the nature of the correspondence *between layers*. In fact, the parameter ω_i in function F_{ω_i} at layer 1 is itself a function of time which depends on the dynamical state y_i of node i at layer 2, while the parameter χ_i at layer 2 depends on the state x_i of node i at layer 1. Namely, we have:

$$\begin{cases} \dot{\omega}_i = f(\omega_i, y_i) \\ \dot{\chi}_i = g(\chi_i, x_i) \end{cases} \qquad i = 1, 2, \dots N \tag{2}$$

where f and g are two assigned functions.

As a specific example of this type of coupling, and of the phenomena that can emerge out of it, we study a toy model of the human brain. Neural systems depend on the combination of several dynamics, including

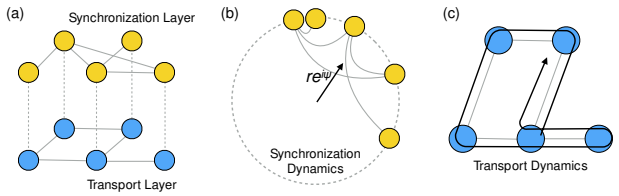

FIG. 1. **Intertwined dynamical processes.** (a) An example of a two-layer multiplex of $N = 5$ nodes with neural synchronization dynamics at layer 1 (top), and transport dynamics at layer 2 (bottom). (b) The neural activity is described by the Kuramoto model in Eq. (3), and the degree of synchronization is measured by the order parameter r. (c) The transport dynamics is modelled by biased random walkers moving according to Eq. (4). The two dynamical processes are bidirectionally coupled, as the natural frequencies of the oscillators at layer 1 depend on the distribution of random walkers at layer 2 and, at the same time, the random walkers are biased on the degree of synchronization of the nodes at layer 1, as described in Eqs. (5)–(6).

blood flow, oxygen exchange, chemical and electrical interactions among neurons, and remote synchronization of distant regions [20–23]. Our multiplex network approach here wants to mimic the interplay between neural activity and energy transport across brain regions as illustrated in Figure 4(a). Neural activity at the level of brain regions is modelled by the Kuramoto model [24], such that the state $x_i(t) \in [0, 2\pi)$ of node i at layer 1 corresponds to the phase of oscillator i at time t, and the first of Eqs. (1) reads:

$$\dot{x}_i = \omega_i + \lambda \sum_{j=1}^{N} a_{ij}^{[1]} \sin(x_j - x_i), \tag{3}$$

where ω_i corresponds to the natural frequency of the oscillator i and λ is the *coupling strength*. The degree of global synchronization in the neural activity is measured by the Kuramoto order parameter $0 \leq r \leq 1$ defined by the complex number $re^{\mathrm{i}\psi} = \frac{1}{N}\sum_{j=1}^{N} e^{\mathrm{i}x_j}$ which represents the centroid of all the oscillators on the complex plane. The second dynamical process, namely energy transport at the second layer, is modelled by a continuous-time random walk [25]. Specifically, the state $y_i(t) \in [0, 1]$ at time t of node i at the transport layer is equal to the fraction of random walkers at node i at time t, and the second of Eqs. (1) reads:

$$\dot{y}_i = \frac{1}{\tau_y} \sum_{j=1}^{N} (\pi_{ij} - \delta_{ij})\, y_j = \frac{1}{\tau_y} \sum_{j=1}^{N} \left(\frac{a_{ji}^{[2]} \chi_i^{\alpha}}{\sum_l a_{jl}^{[2]} \chi_l^{\alpha}} - \delta_{ij} \right) y_j \tag{4}$$

where π_{ij} is the transition probability from node j to node i, τ_y is the time scale of the random walker dynamics, and we have assumed that the random walk is biased on a node property χ_i, with a tuneable *bias exponent* α [26–29]. Notice that for $\alpha > 0$ (resp., $\alpha < 0$) the walkers will preferentially move towards nodes characterised by high (resp., low) values of χ, while for $\alpha = 0$ we recover the standard unbiased random walk.

To define completely the model, we have to specify how the neural dynamics and the diffusion of nutrients are coupled, i.e. we need to assign the functions f and g in Eqs. (2) respectively relating the frequency ω_i of the oscillator i at layer 1 to the available resource y_i at layer 2, and the bias property χ_i of the random walkers at layer 2 to the oscillator phase x_i at layer 1. First, we assume that the natural frequencies ω_i, $i = 1, 2, \ldots, N$, evolve dynamically relaxing to values proportional to the fraction of random walkers at node i in the transport layer:

$$\dot{\omega}_i = \frac{1}{\tau_\omega} \left(N y_i(t) - \omega_i \right), \tag{5}$$

where τ_ω gives the timescale for the relaxation. This choice is motivated by the fact that firing at a higher frequency usually requires a correspondingly higher amount of energy, in the form of oxygen and nutrients carried by blood [30]. Next, we assume that the quantities χ_i evolve according to:

$$\dot{\chi}_i = \frac{1}{\tau_\chi} \left(s_i^{\mathrm{dyn}} - \chi_i \right). \tag{6}$$

where s_i^{dyn} is the dynamic strength of node i, which measures the local degree of synchronization of oscillator i (degree to which i is synchronized with its neighbors) and is defined as $s_i^{\mathrm{dyn}} = r_i \cos(\psi_i - x_i)$ in terms of the local synchronization order parameter $r_i e^{\mathrm{i}\psi_i} = \sum_j a_{ij}^{[1]} e^{\mathrm{i}x_j}$. In this way χ_i relaxes to the dynamic strength of oscillator i with a timescale τ_χ, and therefore the random walk described by the transition probabilities in Eq. (4) is biased towards (away from) strongly-synchronized nodes for positive (negative) values of α. This choice is supported by empirical studies confirming the existence of correlations between the electrical activity of a brain area and the hematic inflow in the same area, which is responsible for the transport of energy to the neurons in the form of oxygen molecules. In particular, it has been suggested that the high electrical activity of a brain area is normally followed by an increase in the blood inflow in the same area [31–33].

Summing up, in the model in Eqs. (3-6) the firing rate of a given node i depends on the availability of energy at i at the transportation layer, and vice versa the abundance of nutrients at node i depends on the local synchronization of oscillator i at the neural dynamics layer. Our model has two control parameters, λ and α, that we can change to tune respectively the coupling between oscillators at layer 1 and the strength of the bias in the random walk at layer 2. To illustrate the effects of intertwining the two dynamical processes, we consider a multiplex network with $N = 1000$ nodes whose synchronization layer is a scale-free (SF) graph [34] with degree

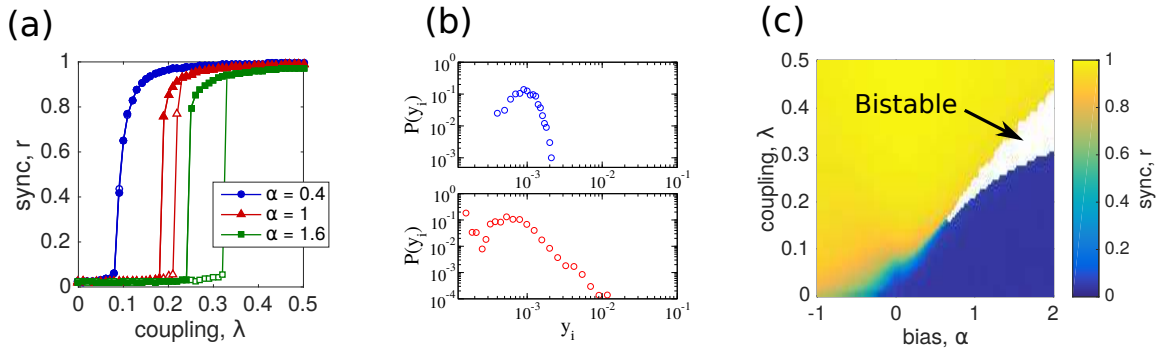

FIG. 2. **Spontaneous explosive synchronization induced by the multiplex coupling of the two processes**. (a) Level of synchronization r vs λ at layer 1 for bias exponents $\alpha = 0.4$, 1.0, and 1.6 (blue, red, and green, respectively). (b) Distribution $P(y_i)$ of steady-state random walker fractions y_i at layer 2 for $\alpha = 1.0$, when the oscillators at layer 1 are incoherent ($\lambda = 0.1$, top, blue) and synchronized ($\lambda = 0.4$ bottom, red). (c) Synchronization phase diagram showing r as a function of coupling λ and bias exponent α. The bistable region is colored in white. Networks are of size $N = 1000$ with $\gamma = 3$ and $\langle k^{[1]} \rangle = \langle k^{[2]} \rangle = 10$.

distribution $P\left(k^{[1]}\right) \propto \left(k^{[1]}\right)^{-\gamma}$ with $\gamma = 3$ above a minimum degree $k_0^{[1]}$, and whose transport layer is a Erdős-Rényi (ER) random graph [35] with link probability p. The average degrees of the two layers are thus given by $\langle k^{[1]} \rangle = \frac{\gamma-1}{\gamma-2} k_0^{[1]}$ and $\langle k^{[2]} \rangle = p(N-1)$. We choose a SF graph for the synchronization layer given the prevalence of such topologies in real neural systems [36], and we have considered the limits $\tau_y, \tau_\omega, \tau_\chi \to 0^+$ corresponding to instantaneous relaxation, meaning the relaxation dynamics of Eqs. (4), (5) and (6) is faster compared to the dynamics of the oscillators. These fast relaxation timescales have been chosen for simplicity, and we note that the phenomena we present here persists for finite values of τ_y, τ_ω, and τ_χ, as we show in the Supplementary Information.

We simulated the model on networks with $\langle k^{[1]} \rangle = \langle k^{[2]} \rangle = 10$, by adiabatically increasing and then decreasing the coupling strength λ at fixed values of the bias parameter α. In Figure 5(a) we report the synchronization profiles r vs λ for $\alpha = 0.4$, 1.0, and 1.6 (blue circles, red triangles, and green squares respectively) at layer 1. Notice that for $\alpha = 0.4$ we have the typical continuous phase transition of the Kuramoto model. Conversely, for $\alpha = 1.0$ and 1.6 we observe the emergence of a switch-like *explosive synchronization* [37] and a bistability in the form of a hysteresis loop (in the forward and backward branches of the profiles). In Figure 5(b) we focus on layer 2, and we plot the distribution $P(y_i)$ of the steady-state random walker occupation probabilities y_i for $\alpha = 1$, corresponding respectively to $\lambda = 0.1$ when the system at layer 1 is in an incoherent state (top, blue), and to $\lambda = 0.4$ when the system at layer 2 is synchronized (bottom, red). While the values of y_i are relatively homogeneous in the incoherent state and span less than a decade, in the synchronized state the distribution is heterogeneous and spanning several decades. Finally, in Figure 5(c) we explore the (α, λ) parameter space in more detail, plotting the value of r at layer 1 as a function of the two control parameters of the model. The bistable region which emerges at $\alpha \approx 0.7$ and widens by increasing α is reported in white. We note that this behavior persists under a wide range of network topologies, provided that the synchronization layer is sufficiently heterogeneous, as shown in the Supplementary Information.

Our results indicate that the intertwined nature of diffusion process and synchronization dynamics gives rise to the emergence of phenomena not present if the two dynamics were not coupled. Namely, in the transport layer, we observe a transition from a homogeneous to a heterogeneous distribution of the random walkers throughout the network, according to whether the oscillators at the other layer are incoherent or synchronized. Concurrently, when the random walkers are biased sufficiently strongly towards regions that are more synchronized, the heterogenous distribution of random walkers fosters the emergence of switch-like *explosive synchronization* [37] in the neural dynamics layer. The resulting phase diagram exhibits three phases (incoherent, bistable, and synchronised) and a tricritical point. It is noticeable that explosive synchronization appears naturally in our model due to the intertwined dynamics of the two processes, and it does not require ad hoc externally imposed correlations between the oscillator frequencies and the topology of the interaction network, as those necessary instead in a single layer network with a single dynamics [37, 38].

We now demonstrate that, despite the inherent intricacy of the model, its dynamical behaviour can be understood analytically. In particular, we search for conditions such that random walker probabilities and local order parameters are in a stationary state, $y_i = y_i^*$ and $r_i = r_i^*$. A steady-state analysis can then be carried out for both the transport and synchronization dynamics, which we detail in the Supplementary Information. In particular, we find that the fraction of random walkers y_i^* depends on whether the synchronization dynamics is incoherent

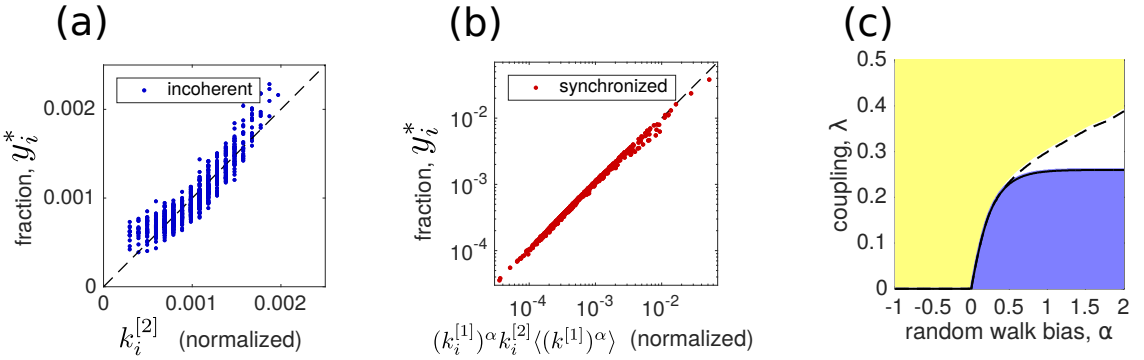

FIG. 3. **Analytical approach to explain the observed collective phenomena.** Fraction y_i of random walkers at node i vs $k_i^{[2]}$ for an incoherent state (a), and vs. $(k_i^{[1]})^\alpha k_i^{[2]} \langle (k^{[1]})^\alpha \rangle$ for a synchronized state. (c) Analytically obtained synchronization phase diagram showing r as a function of λ and α. Networks are of size $N = 1000$ with $\gamma = 3$ and $\langle k^{[1]} \rangle = \langle k^{[2]} \rangle = 10$ as in the numerical simulations shown in Figure 5.

or synchronized, namely:

$$y_i^* \propto \begin{cases} k_i^{[2]} & \text{if } r \approx 0 \\ \left(k_i^{[1]}\right)^\alpha k_i^{[2]} \langle \left(k^{[1]}\right)^\alpha \rangle & \text{if } r \approx 1. \end{cases} \tag{7}$$

Also, the global order parameter r can be written implicitly in terms of the collective frequency $\Omega = \langle \omega \rangle$ and the joint degree-frequency distribution $P(k, \omega)$:

$$r = \frac{1}{\langle k^{[1]} \rangle} \iint\limits_{|\omega - \Omega| \leq \lambda r k^{[1]}} P(k^{[1]}, \omega) k^{[1]} \sqrt{1 - \left(\frac{\omega - \Omega}{\lambda r k^{[1]}}\right)^2} \, d\omega dk^{[1]}, \tag{8}$$

which depends on the topologies of both layers since $\omega_i = N y_i$ in the steady-state. Figure 6 shows that our analytical results are in good agreement with the numerical simulations. In Figures 6(a) and 6(b) we plot the observed fraction y_i of random walkers at the steady state vs the predictions of Eq. (7), respectively for the incoherent and synchronized state. Dashed black lines are plotted to guide the eye. In Figure 6(c) we report the synchronization phase digram obtained from Eq. (8). A comparison with the phase diagram in Figure 5c indicates that our theory is able to accurately reproduce the collective phenomena emerging from the interactions of the two dynamical processes that we have observed in our numerical simulations.

The specific example of intertwined synchronization and transport dynamics studied here shows that interesting collecting behaviors can appear when we couple two dynamical processes taking place on the same set of nodes. Namely, we have found that the distribution of random walkers in the transport network changes from homogeneous to heterogeneous according to whether the synchronization dynamics is incoherent or synchronized, and this result is unexpected since for the topology of the transport network we have on purpose chosen a homogenous graph. At the same time, the heterogeneous distribution of walkers is responsible for the emergence of explosive synchronization, and the appearance of a bistable phase and of a tricritical point in the neural network layer. Importantly, here, explosive synchronization spontaneously emerges from the interactions of the two dynamical processes, without any externally imposed assumptions, necessary instead in networks where the Kuramoto model is not coupled to other dynamical systems [37, 38].

The switch-like transition we have found in our model closely mirrors that displayed by the human brain [22], which has the ability to very quickly switch between resting state activity (i.e., the background activity of a brain when no particular conscious task is performed) and complex intellectual/motor tasks [39], and thus requires a fast and flexible mechanism to induce a sudden and massive synchronization. The choice of this specific model was motivated by the important role that synchronization and transport play in a wide range of natural and man-made systems [40–43] and by the various bistabilities empirically observed in physics, biology and neuroscience [22, 44, 45]. To date, several studies have investigated how a single type of dynamics evolves on a multilayer network [46–49]. However, the framework we have proposed here, based on the use of multiplex networks to mutually couple dynamics of different nature, is very general and versatile. We believe that further studies of other intertwined dynamical processes will uncover other novel phenomena induced by multiplex coupling, and will eventually result in a more thorough understanding of the relation between the structure and the dynamics of multidimensional complex systems.

Appendix A: Derivation of the biased random walk stationary distribution

Here we follow Ref. [26] and derive the stationary distribution of random walkers $\boldsymbol{y}^*$ for the discrete-time version of the motion rule given by Eq. (4) in the main text,

namely:

$$\dot{y}_i = \frac{1}{\tau_y}\left(\sum_{j=1}^{N}\pi_{ij} - \delta_{ij}\right) y_j \tag{A1}$$

where:

$$\pi_{ij} = \frac{a_{ji}^{[2]}\chi_i^\alpha}{\sum_l a_{jl}^{[2]}\chi_l^\alpha} \tag{A2}$$

is the transition probability from node j to node i. We note first that the steady-state solution of Eq. (A1) is given by

$$y_i = \sum_{j=1}^{N}\pi_{ij}y_j = \sum_{j=1}^{N}\frac{a_{ji}^{[2]}\chi_i^\alpha}{\sum_l a_{jl}^{[2]}\chi_l^\alpha}y_j. \tag{A3}$$

Importantly, this steady-state represents the same steady-state of the discrete-time random walk

$$y_i^{t+1} = \sum_{j=1}^{N}\pi_{ij}y_j^t, \tag{A4}$$

which in turn is given by the dominant eigenvector of the transition matrix $\Pi = [\pi_{ij}]$. To find this stationary distribution, we denote $P_{j\to i}(T)$ as the probability of moving from j to i in T discrete time steps, so that

$$P_{j\to i}(T) = \sum_{l_1,l_2,\ldots,l_{t-1}} \pi_{il_{t-1}}\times\pi_{l_{t-1}l_{t-2}}\times\cdots\times\pi_{l_1 j}, \tag{A5}$$

Next, we define the auxiliary parameter $c_j = \sum_{i=1}^{N} a_{ji}^{[2]}\chi_i^\alpha$, and using the symmetry of the network structure (i.e., $a_{ij}^{[2]} = a_{ji}^{[2]}$), it follows that

$$\frac{P_{j\to i}(T)}{P_{i\to j}(T)} = \frac{\chi_i^\alpha c_i}{\chi_j^\alpha c_j}. \tag{A6}$$

Next we look for a stationary state whereby the fraction y_i^* of a walker occupying node i is equal to $P_{l\to i}(T)$ for all l and $T > 0$. Substituting the stationary probabilities and rearranging yields:

$$y_i^*\chi_j^\alpha c_j = y_j^*\chi_i^\alpha c_i. \tag{A7}$$

Summing both sides of Eq. (A7) over j and rearranging, we then obtain

$$y_i^* = \frac{\chi_i^\alpha c_i}{\sum_{j=1}^{N}\chi_j^\alpha c_j} = \frac{\chi_i^\alpha\sum_{l=1}^{N}a_{il}\chi_l^\alpha}{\sum_{j=1}^{N}\chi_j^\alpha\sum_{l=1}^{N}a_{jl}\chi_l^\alpha}. \tag{A8}$$

To complete the analysis, we next assume that the biasing values χ_i evolve according to Equation (6) in the main text and relax to a steady state, defined by $\dot{\chi}_i = 0\ \forall i$. This yields $\chi_i = s_i^*$, where s_i^* represents the steady-state dynamical strength $s_i^{\rm dyn}$ in the synchronization layer as defined by the synchronization dynamics. (We note that such a steady-state value s_i^* is valid provided that the network is large enough so that finite-size fluctuations remain sufficiently small). Since the steady-state dynamical strength is defined as $s_i^* = r_i^*\cos(\psi_i^* - x_i^*)$ we have two cases. If the oscillator dynamics are incoherent then $r_i \approx 0$. Moreover, any finite system exhibits finite-size fluctuations around the incoherent state, so we can approximate $r_i \approx \xi$ for some $\xi \ll 1$, yielding $\chi_i^* \approx$ constant. On the other hand, if the oscillator dynamics are synchronized then $r_i^* \approx k_i^{[1]}r^*$ and we can approximate $\chi_i^* \approx rk_i$. Inserting these expressions into Eq. (A8) we finally obtain:

$$y_i^* \propto \begin{cases} k_i^{[2]} & \text{if } r\approx 0 \\ \left(k_i^{[1]}\right)^\alpha k_i^{[2]}\langle\left(k^{[1]}\right)^\alpha\rangle & \text{if } r\approx 1, \end{cases} \tag{A9}$$

as in Equation (7) in the main text.

Appendix B: Derivation of the synchronization self-consistency equation

Here we derive the self consistency condition given in Eq. (8) of the main text, strarting from the governing synchronization dynamics in Eq. (3) of the main text and using a heterogeneous mean-field approach. In particular, we will approximate the entries of the adjacency matrix A using nodal degrees, specifically

$$a_{ij}^{[1]} \approx \frac{k_i^{[1]}k_j^{[1]}}{N\langle k^{[1]}\rangle}, \tag{B1}$$

where $\langle k^{[1]}\rangle = N^{-1}\sum_j k_j^{[1]}$ is the mean degree in the synchronization layer. We also introduce a modified order parameter,

$$\tilde{r}e^{\mathrm{i}\tilde{\psi}} = \frac{1}{N\langle k^{[1]}\rangle}\sum_{j=1}^{N}k_j^{[1]}e^{\mathrm{i}x_j}, \tag{B2}$$

which is similar to the typical order parameter, except for a re-weighting of the angles according to degree. We note that, just like r, the modified order parameter $\tilde{r}$ varies between zero and one, and tends to be a very strong approximation to r. We introduce the modified order parameter because of its utility in the analysis of the synchronization dynamics. Along with the mean-field approximation of A [i.e., Eq. (B1)], Eq. (B2) allows us to simplify the governing dynamics in the synchronization layer to

$$\dot{x}_i = \omega_i + \lambda\tilde{r}k_i^{[1]}\sin(\tilde{\psi} - x_i). \tag{B3}$$

We note that the accuracy of this mean-field approximation improves as the network topology becomes denser, which is why we use a relatively dense network with mean degree $\langle k\rangle = 10$ in the main text.

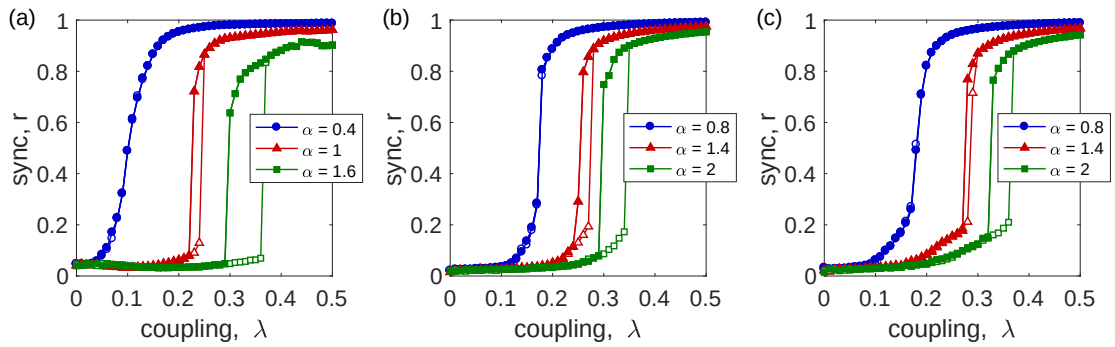

FIG. 4. **Finite Time Scale Dynamics I.** Synchronization profiles of the degree of synchronization r vs the coupling strength λ with a few different biasing parameters α for finite relaxation time scales: (a) $\tau_y, \tau_\omega, \tau_\chi = 10^{-2}$, (b) $\tau_y = 10^{-2}$ and $\tau_\omega, \tau_\chi = 10^{-1}$, and (c) $\tau_y, \tau_\omega, \tau_\chi = 10^{-1}$.

Next, we look for a synchronized state by first noting that for a strongly synchronized population, where each oscillator becomes entrained, the collective frequency Ω of the population is given by the mean natural frequency, i.e., $\Omega = \langle\omega\rangle = N^{-1}\sum_j \omega_j$. Thus, an oscillator that becomes entrained with the rest of the population evolves with a velocity of $\dot{x}_i = \Omega$. After entering the appropriate rotating frame $x_i \mapsto x_i + \Omega t$ and inspecting Eq. (B3), it is easy to see that an oscillator i becomes entrained, or locked, if and only if it satisfies

$$|\omega_i - \Omega| \leq \lambda \tilde{r} k_i^{[1]}, \tag{B4}$$

and otherwise it continually "drifts" past the synchronized population. In particular, a locked oscillator i then comes to equilibrium at

$$x_i = \arcsin\left(\frac{\omega_i - \Omega}{\lambda \tilde{r} k_i^{[1]}}\right). \tag{B5}$$

To classify the degree of synchronization we inspect the modified order parameter $\tilde{r}e^{i\tilde{\psi}}$. First, we note that with a suitable shift of initial conditions we may set the mean angle $\psi = 0$, so expanding the exponential and keeping the real part (since the imaginary part must be zero) yields

$$\tilde{r} = \frac{1}{N\langle k^{[1]}\rangle}\sum_{j=1}^{N} k_j^{[1]} \cos x_j. \tag{B6}$$

Neglecting the effect of drifting oscillators on the order parameter, we sum over the locked population and insert Eq. (B5) into Eq. (B6) to obtain

$$\tilde{r} = \frac{1}{N\langle k^{[1]}\rangle}\sum_{|\omega_j - \Omega| \leq \lambda \tilde{r} k_j^{[1]}} k_j^{[1]} \sqrt{1 - \left(\frac{\omega_j - \Omega}{\lambda \tilde{r} k_j^{[1]}}\right)^2}. \tag{B7}$$

Finally, for large networks the sum in Eq. (B7) can be converted to an integral using the joint distribution $P(k^{[1]}, \omega)$:

$$\tilde{r} = \frac{1}{\langle k^{[1]}\rangle}\iint_{|\omega - \Omega| \leq \lambda \tilde{r} k^{[1]}} P(k^{[1]}, \omega) k^{[1]} \sqrt{1 - \left(\frac{\omega - \Omega}{\lambda \tilde{r} k^{[1]}}\right)^2}\, d\omega dk^{[1]}, \tag{B8}$$

Finally, we arrive at Eq. (8) in the main text after approximating $r \approx \tilde{r}$. We note that this approximation holds extremely well for networks with homogeneous degree distributions, but in principle can lose accuracy as the degree distribution becomes more and more heterogeneous, since $\tilde{r}$ represents a convenient re-weighting of the terms that contribute to r. We find in practice, however, that the two values are remarkably close due to the fact that, if a system synchronizes strongly as we see in our system, the re-weighting has little effect.

Appendix C: Finite relaxation dynamics

Here we present numerical results for the cases of finite relaxation time scales for the random walker, natural frequency, and bias variables given by τ_y, τ_ω, and τ_χ in Eqs. (4), (5), and (6), respectively, in the main text. Recall that the main results presented in the main text considered the limit of quick relaxation, i.e., $\tau_y, \tau_\omega, \tau_\chi \to 0^+$. Here we demonstrate that the novel phenomenon we observe in the system is not restricted to this particular choice. We begin by considering a few different choices of time scales and focus on the synchronization dynamics. In Figure 4 we plot the resulting synchronization profiles for the degree of synchronization r vs the coupling strength λ with a few different values of the bias parameter α for a few different choices of time scales. In panel (a) we choose all $\tau_y, \tau_\omega, \tau_\chi = 10^{-2}$, in panel (b) we choose $\tau_y = 10^{-2}$ and $\tau_\omega, \tau_\chi = 10^{-1}$, and in panel (c) we choose all $\tau_y, \tau_\omega, \tau_\chi = 10^{-1}$. Results use networks of size $N = 1000$ with SF ($\gamma = 3$) and ER topologies in the synchronization and transport layers, respectively,

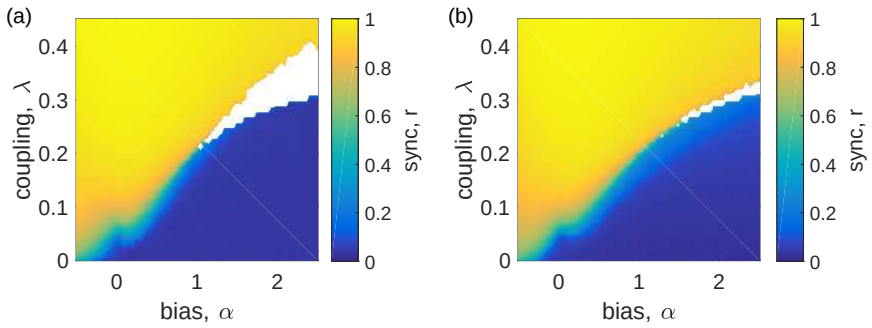

FIG. 5. **Finite Time Scale Dynamics II.** Stability diagrams obtained numerically for the (α, λ) parameter space using finite relaxation time scales. The order parameter r is color coded blue and yellow for $r = 0$ and $r = 1$, respectively, with different relaxation time scales: (a) $\tau_y, \tau_\omega, \tau_\chi = 10^{-2}$ and (b) $\tau_y, \tau_\omega, \tau_\chi = 10^{-1}$.

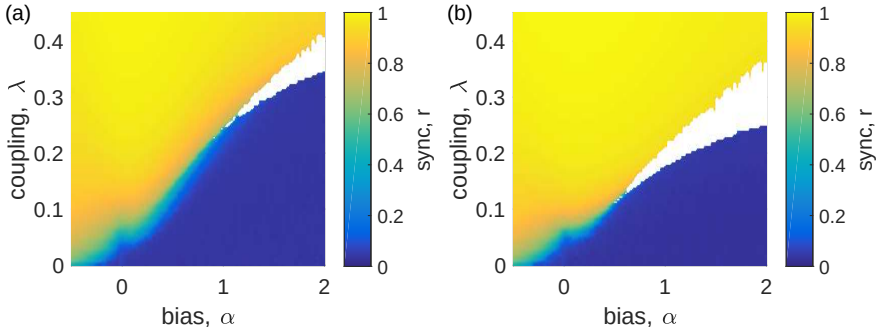

FIG. 6. **Effect of Network Topology I.** Stability diagrams obtained numerically for the (α, λ) parameter space using various network topologies. The order parameter r is color coded blue and yellow for $r = 0$ and $r = 1$, respectively, with SF network topology in the synchronization layer with exponents (a) $\gamma = 2.6$ and (b) 3.4, and ER network topology in the transport layer. In both cases the mean degree in each layer is $\langle k \rangle = 10$.

each with mean degree $\langle k \rangle = 10$. In each case we observe qualitatively similar behavior as those results presented in the main text, i.e., a second order, continuous transition between incoherence and synchronization for smaller α values and the emergence of a first-order explosive transition between incoherence and synchronization for larger α values. While the results remain qualitatively similar, we make note of a quantitative difference: as the relaxation dynamics become slower, i.e., the time scales become larger, a larger value of α is required for explosive synchronization to emerge. We also note that when the time scales become sufficiently large we observe that explosive synchronization does not occur spontaneously.

To accompany these results we explore the (α, λ) parameter space more thoroughly, presenting the numerically-obtained stability diagram for the system with finite relaxation time scales. In particular, in Figure 5 we plot the steady-state degree of synchronization r found as a function of both α and λ. Results are color coded so that $r = 0$ and $r = 1$ are given by blue and yellow, respectively, and regions where both incoherent and synchronized states are found to be stable are given by the white regions. In panels (a) and (b) we plot the results for time scale choices $\tau_y, \tau_\omega, \tau_\chi = 10^{-2}$ and $\tau_y, \tau_\omega, \tau_\chi = 10^{-1}$, respectively. Results use networks of size $N = 500$ with SF ($\gamma = 3$) and ER topologies in the synchronization and transport layers, respectively, each with mean degree $\langle k \rangle = 10$. Here we can more clearly see the emergence of a bistable regime for a large enough α value. Moreover, we see that a faster relaxation time scale leads to a larger bistable region.

Appendix D: Effect of Network Topology

Here we present numerical results that explore the effect of using different network topologies than those presented in the main text, where we assumed a SF topology in the synchronization layer with exponent $\gamma = 3$ and an ER topology in the transport layer. In particular, we show that the results we presented in the main text are qualitatively reproduced for different topologies. We begin by varying the heterogeneity in the synchronization layer via the exponent γ. In Fig. 6 we present the stability diagrams for the synchronization dynamics for (a) a more heterogeneous topology in the synchronization layer obtained by using $\gamma = 2.6$ and (b) a less heterogeneous topology in the synchronization layer obtained by using

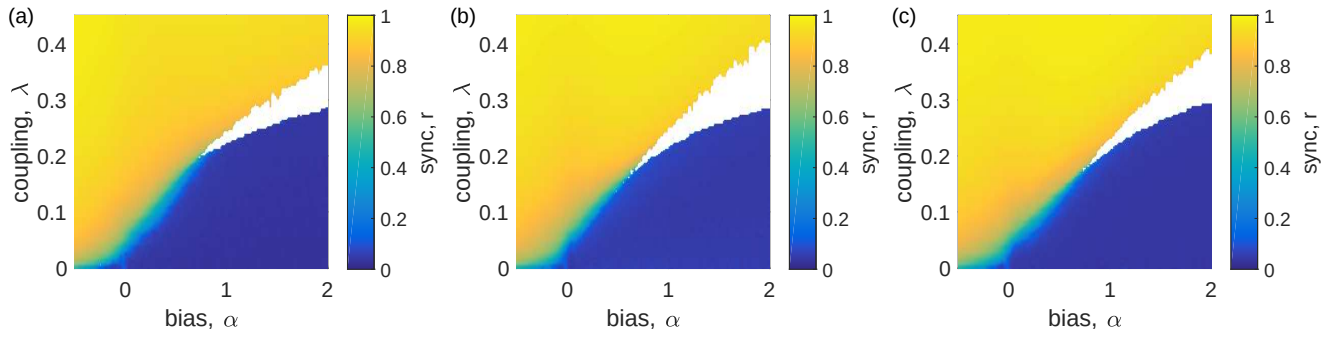

FIG. 7. **Effect of Network Topology II.** Numerically obtain stability diagram for the (α, λ) parameter space using various network topologies. The order parameter r is color coded blue and yellow for $r = 0$ and $r = 1$, respectively, with SF network topology in the synchronization layer with exponent $\gamma = 3.0$ and SF network topology in the transport layer with exponents (a) $\gamma = 2.6$, (b) 3, and (c) 3.4. In each case the mean degree in each layer is $\langle k \rangle = 10$.

$\gamma = 3.4$. In both cases, the topology of the transport layer is ER and both layers have mean degree $\langle k \rangle = 10$. As in previous stability diagrams, we plot the steady-state degree of synchronization r found as a function of both α and λ. Results are color coded so that $r = 0$ and $r = 1$ are given by blue and yellow, respectively, and regions where both incoherent and synchronized states are found to be stable are given by the white regions. We note that in both cases bistability persists, indicating the existence of explosive synchronization for sufficiently strong bias in the random walker dynamics.

Moreover, we also explore the possibility where both networks have SF topologies. In Fig. 6 we present the stability diagrams for the case where the synchronization layer has an SF topology with $\gamma = 3$ while the transport layer has SF topologies with varying degrees of heterogeneity: (a) $\gamma = 2.6$, (b) $\gamma = 3$, and (c) $\gamma = 3.4$. In each case, both layers have mean degree $\langle k \rangle = 10$. Again, as in previous stability diagrams, we plot the steady-state degree of synchronization r found as a function of both α and λ. Results are color coded so that $r = 0$ and $r = 1$ are given by blue and yellow, respectively, and regions where both incoherent and synchronized states are found to be stable are given by the white regions. We point out that bistability persists in each case, indicating the existence of explosive synchronization for sufficiently strong bias in the random walker dynamics.

ACKNOWLEDGMENTS

A.A. and S.S. acknowledge support from MULTIPLEX, grant number 317532 of the European Commission. V.L. and V.N. acknowledge support from LASAGNE, grant number 318132 funded by the European Commission. V.L. acknowledge support from the EPSRC projects GALE, EP/K020633/1, and EP/N013492/1. A.A. acknowledges Spanish Ministerio de Economiia y Competitividad, grant number FIS2015-71582-C2-1, ICREA Academia and the James S. McDonnell Foundation.

[1] S. H. Strogatz, Exploring complex networks. *Nature* **410**, 268–276 (2001).
[2] M. E. J. Newman, The structure and function of complex networks. *SIAM Rev.* **45**, 167–256 (2003).
[3] F. Dörfler, M. Chertkov, F. Bullo, Synchronization in complex oscillator networks and smart grids. *Proc. Natl. Acad. Sci. U.S.A.* **110**, 2005–2010 (2013).
[4] R. Pastor-Satorras, A. Vespignani, Epidemic spreading in scale-free networks. *Phys. Rev. Lett.* **86**, 3200 (2001).
[5] J. D. Noh, H. Rieger, Random walks on complex networks. *Phys. Rev. Lett.* **92**, 118701 (2004).
[6] D. B. Larremore, W. L. Shew, J. R. Restrepo, Predicting criticality and dynamic range in complex networks: effects of topology. *Phys. Rev. Lett.* **106**, 058101 (2011).
[7] S. Boccaletti, V. Latora, Y. Moreno, M. Chavez, D. U. Hwang, Complex networks: structure and dynamics. *Phys. Rep.* **424**, 175–308 (2006).
[8] A. Arenas, A. Díaz-Guilera, J. Kurths, Y. Moreno, C. & Zhou, Synchronization in complex networks. *Phys. Rep.* **469**, 93–153 (2008).
[9] T. Nishikawa, A. E. Motter, Y.-C Lai, F. C. Hoppensteadt, Heterogeneity in oscillator networks: are smaller worlds easier to synchronize? *Phys. Rev. Lett.* **91**, 014101 (2003).
[10] A. Arenas, A. Díaz-Guilera, C. J. Pérez-Vicente, Synchronization reveals topological scales in complex networks. *Phys. Rev. Lett.* **96**, 114102 (2006).
[11] M. Rosvall, C. T. & Bergstrom, Maps of random walks on complex networks reveal community structure. *Proc. Natl. Acad. Sci.* **105**, 1118–1123 (2008).
[12] V. Nicosia, M. De Domenico, V. Latora, Characteristic exponents of complex networks. *Europhysics Letters* **106**, 58005 (2014).
[13] S. V. Buldyrev, R. Parshani, G. Paul, H. E. Stanley, S.

& Havlin, Catastrophic cascade of failures in interdependent networks. *Nature* **464**, 1025–1028 (2010).
[14] C. Granell, S. Gomez, A. Arenas, Dynamical interplay between awareness and epidemic spreading in multiplex networks. *Phys. Rev. Lett.* **111**, 128701 (2013).
[15] A. Czaplicka, R. Toral, M. San Miguel, Competition of simple and complex adoption on multi-layer networks, arXiv:1605.03479.
[16] M. De Domenico et al., Mathematical Formulation of Multilayer Networks *Phys. Rev. X* **3**, 041022 (2013).
[17] M. Kivelä et al., Multilayer networks. *J. Complex Netw.* **2**, 203–271 (2014).
[18] S. Boccaletti et al., The structure and dynamics of multilayer networks, *Phys. Rep.* **544**, 1 (2014).
[19] F. Battiston, V. Nicosia, V. Latora Structural measures for multiplex networks *Phys. Rev. E.* **89,** (3) 032804 (2014).
[20] F. Varela, J.-P. Lacjaux, E. Rodriguez, J. Martinerie, The brainweb: Phase synchronization and large-scale integration. *Nat. Rev. Neurosci.* **2**, 229–239 (2001).
[21] E. Bullmore, O. Sporns, Complex brain networks: graph theoretical analysis of structural and functional systems, *Nat. Rev. Neurosci.* **10**, 186 (2009).
[22] G. Deco, V. K. Jirsa, A. R. McIntosh, Resting brains never rest: computational insights into potential cognitive architectures. *Trends. Neurosci.* **36**, 268–274 (2013).
[23] V. Nicosia, M. Valencia, M. Chavez, A. Díaz-Guilera, V. Latora, Remote synchronization reveals network symmetries and functional modules, *Phys. Rev. Lett.* **110**, 174102 (2013).
[24] Y. Kuramoto, Y. Chemical Oscillations, Waves, and Turbulence (Springer, 1984).
[25] R. Lambiotte, J.-C. Delvenne, M. Barahona, Laplacian Dynamics and Multiscale Modular Structure in Networks. arXiv:0812.1770
[26] J. Gómez-Gardeñes, V. & Latora, Entropy rate of diffusion processes on complex networks. *Phys. Rev. E* **78**, 065102(R) (2008).
[27] R. Sinatra, J. Gomez-Gardenes, R. Lambiotte, V. Nicosia, V. Latora, Maximal-entropy random walks in complex networks with limited information, *Phys. Rev. E* **83**, 030103(R) (2011).
[28] R. Lambiotte, R. Sinatra, J.-C. Delvenne, T. S. Evans, M. Barahona, V. Latora, Flowgraphs: Interweaving dynamics and structure. *Phys. Rev. E* **84**, 017102 (2011).
[29] F. Battiston, V. Nicosia, V. Latora, Efficient exploration of multiplex networks, *New J. Phys.* **18**(4), 043035 (2016).
[30] L. Edvinsson, D. N. Krause (Eds). *Cerebral Blood Flow and Metabolism, 2nd Edition* (Williams & Wilkins, Philadelphia, 2002).
[31] D. Malonek et al., Vascular imprints of neuronal activity: Relationships between the dynamics of cortical blood flow, oxygenation, and volume changes following sensory stimulation, *Proc. Natl. Acad. Sci. USA* **94**(26), 14826 (1997).
[32] S. A. Sheth et al., Linear and nonlinear relationships between neuronal activity, Oxygen metabolism, and hemodynamic responses, *Neuron* **42**(2), 347 (2004).
[33] E. A. Allen, B.N. Pasley, T. Duong, R. D. Freeman, Transcranial magnetic stimulation elicits coupled neural and hemodynamic consequences, *Science* **317**(5846), 1918 (2007).
[34] M. Molloy, B. Reed, Critical point for random graphs with a given degree sequence. *Random Struct. Algor.* **6**, 161–180 (1995).
[35] P. Erdős, A. Rényi, On the evolution of random graphs. *Publ. Math. Inst. Hung. Acad. Sci.* **5**, 17–61 (1960).
[36] V. M. Eguíluz, D. R. Chialvo, G. A. Cecchi, M. Baliki, A. V. Apkarian, Scale-Free Brain Functional Networks. *Phys. Rev. Lett.* **94**, 018102 (2005).
[37] J. Gómez-Gardeñes, S. Gómez, A. Arenas, Y. Moreno, Explosive synchronization transitions in scale-free networks. *Phys. Rev. Lett.* **106**, 128701 (2011).
[38] I. Leyva et al., Explosive transitions to synchronization in networks of phase oscillators. *Sci. Rep.* **3**, 1281 (2013).
[39] M. E. Raichle et al., A default mode of brain function, *Proc. Natl. Acad. Sci. USA* **98**, 676 (2001).
[40] J. G. Restrepo, E. Ott, B. R. Hunt, Onset of synchronization in large networks of coupled oscillators. *Phys. Rev. E* **71**, 036151 (2005).
[41] A. E. Motter, S. A. Myers, M. Anghel, T. Nishikawa, Spontaneous synchrony in power-grid networks. *Nat. Phys.* **9**, 191–197 (2013).
[42] P. S. Skardal, A. Arenas, Control of coupled oscillator networks with application to microgrid technologies. *Sci. Adv.* **1**, e1500339 (2015).
[43] D. F. Gleich, PageRank beyond the web. *SIAM Rev.* **57**, 321–363 (2015).
[44] E. A. Martens, S. Thutupalli, A. Fourrière, O. Hallatschek, Chimera states in mechanical oscillator networks. *Proc. Natl. Acad. Sci. U.S.A.* **110**, 10563–10567 (2013).
[45] O. Brandman, J. E. Ferrell, R. Li, T. Meyer, Interlinked fast and slow positive feedback loops drive reliable cell decisions. *Science* **310**, 496–498 (2005).
[46] F. D. Sahneh and C. Scoglio, Competitive epidemic spreading over arbitrary multilayer networks. *Phys. Rev. E* **89**, 062817 (2014).
[47] K.-M. Lee, C. D. Brummitt, and K.-I. Goh, Threshold cascades with response heterogeneity in multiplex networks. *Phys. Rev. E* **90**, 062816 (2014).
[48] M. Pósfai, J. Gao, S. P. Cornelius, A.-L. Barabási, and R. M. D'Souza, Controllability of multiplex, multi-timescale networks. *Phys. Rev. E* **94**, 032316 (2016).
[49] R. Burkholz, M. V. Leduc, A. Garas, and F. Schweitzer, Systemic risk in multiplex networks with asymmetric coupling and threshold feedback. *Physica D* **323-324**, 64–72 (2016).